

Unsteady Propulsion by an Intermittent Swimming Gait

By EMRE AKOZ¹ AND KEITH W. MOORED,¹

¹Department of Mechanical Engineering and Mechanics
Lehigh University, Bethlehem, PA 18015, USA

(Received December 3, 2024)

Computational results are presented on comparison of intermittently and continuously pitching two dimensional airfoils. In literature, a viscous mechanism proposed by Lighthill (1971) where skin friction of an undulating body can be around 3 – 5 times greater than a rigidly-held coasting body, has been the well adopted explanation of energetic advantage of the intermittent gait over continuous gait. We find that in an inviscid environment, with only involvement of pressure forces, up to 60% of energy is saved by using intermittent swimming. The maximum economy benefit is observed with modified Strouhal number range of 0.15 – 0.5 and the reduced frequency range of 2 – 5. The inviscid mechanism that leads to the superior performance is observed to be coming from the increase of the ratio of thrust generating forces to the induced drag forces. This increase happens as the ratio of swimming to coasting duration is adjusted. In addition, scaling laws predicting the thrust, power, free swimming velocity and cost of transport of two dimensional continuously pitching airfoils are studied for the intermittent swimming gait.

1. Introduction

Many fish such as haddock (Harden-Jones pres. comm.), cod (Videler 1981), saithe (Videler & Weihs 1982), zebra danios (Müller *et al.* 2000), cormorant (Ribak *et al.* 2005) and koi carps (Wu *et al.* 2007) swim by using a combination of an active swimming phase and a passive coasting phase known as burst-and-coast or burst-and-glide swimming. This intermittent swimming gait adopted by fish, has been predicted by dynamical models to yield an energy savings to swim a given distance of over 50% (Weihs 1974, 1980). These predictions are based on the Bone-Lighthill boundary layer thinning hypothesis, which proposes that there is an increase in skin friction drag on a fish body when it undulates (Lighthill 1971). The skin friction increase is caused by the thinning of the boundary layer from the body normal velocity component that is present during undulation. In fact, Lighthill originally estimated that the skin friction drag on a swimming body can be up to a factor of 5 times larger than a gliding body (Lighthill 1971). Others estimated that the factor could be in a range of 4-10 (Webb 1975; Videler 1981; Wu *et al.* 2007). More recently, detailed analysis confirms the boundary layer thinning hypothesis, but estimates the skin friction drag increase to be much more modest than originally proposed and in the range of a 20–90% drag increase (Ehrenstein & Eloy 2013; Ehrenstein *et al.* 2014).

Given this range of skin friction increase, the viscous mechanism proposed by Bone and Lighthill (1971) is not sufficient to create a 50% savings in energy by itself. Yet, a 45% energy savings was indirectly estimated from DPIV experiments that measured the thrust impulse imparted to the wake of koi carps (Wu *et al.* 2007). Also, a 56%

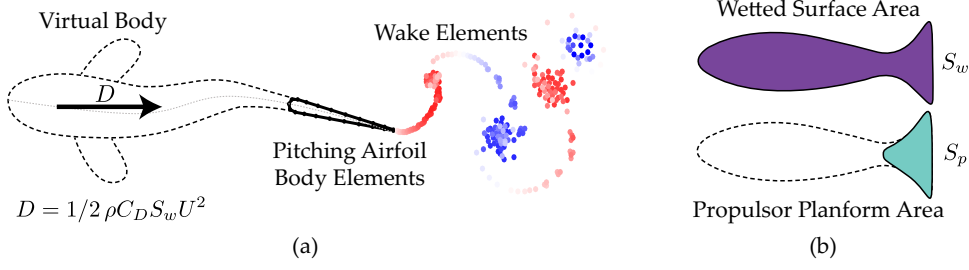


FIGURE 1. (a) The schematic of the idealized self-propelled swimmer. Dashed line represents the virtual body. There is a drag force, D , acting on the hydrofoil that represents the virtual body. The wake element end points are colored red and blue for counter clockwise and clockwise circulation, respectively. (b) S_w is the wetted surface area of a generic swimmer and represented by the purple color. S_p is the propulsor area and represented by the blue color. $S_{wp} = S_w/S_p$.

energy savings for an intermittent fish-like swimmer was directly calculated by using a two-dimensional Navier-Stokes solver (Chung 2009).

Motivated by these observations, we hypothesize that there is an inviscid mechanism that can account for the majority of the energetic benefit seen in intermittent swimming for parameters typical of biology. To examine this hypothesis, we show that by using inviscid computations there is an energy savings for intermittent swimming as compared to continuous swimming at the same swimming speed. Then we consider three questions: What is the nature of the inviscid mechanism that leads to the observed energy savings, how do the forces and energetics of intermittent swimming scale with the swimming parameters, and what are the limitations to the benefit?

2. Approach and Numerical Methods

2.1. Problem Formulation and Input Parameters

A computational study is performed to compare the performance and flow fields of idealized continuous and intermittent swimmers. A self-propelled swimmer that is a combination of a virtual body and a two-dimensional hydrofoil pitching about its leading edge is used to model the problem (Figure 1a). The virtual body is not present in the computational domain, however, its presence is modeled as a drag force, D , that acts to resist the motion of the swimmer. The magnitude of the drag force is determined from a drag law based on high Reynolds number swimming conditions (Munson 1990),

$$D = 1/2 \rho C_D S_w U^2$$

where ρ is the density of the fluid, C_D is the coefficient of drag of the virtual body, S_w is the combined wetted surface area of the virtual body and the propulsor (Figure 1b), and U is the cruising speed of the swimmer. The planform area of the hydrofoil, S_p , is defined as the chord length, c , multiplied by a unit span length. The chord length is fixed to $c = 0.07$ m, which is typical of species that use intermittent swimming gaits (Beamish 1966; Videler 1981). An area ratio can then be formed as the ratio of the wetted surface area to the propulsor planform area,

$$S_{wp} \equiv \frac{S_w}{S_p}.$$

The area ratio, used to calculate S_w in the drag law, is selected to be $S_{wp} = 8$, which is typical for intermittently swimming species (Beamish 1966; Videler 1981; Videler & Wardle

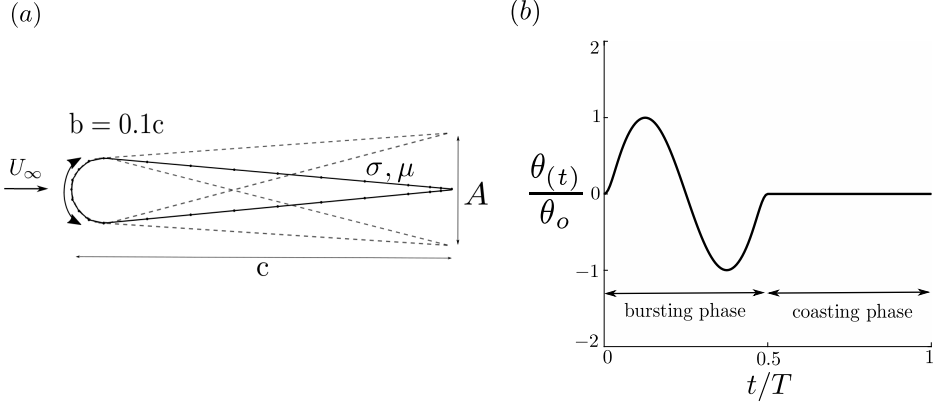


FIGURE 2. (a) Geometric and numerical parameters for the teardrop hydrofoil. (b) Normalized pitching angle as a function of normalized time for an intermittent swimmer with $DC = 0.5$.

1991; Webber *et al.* 2001). In addition, the pitching hydrofoil has a teardrop cross-sectional shape (Marais *et al.* 2012) with a thickness to chord ratio of $b/c = 0.1$ (see Figure 2a).

Previous analytic and computational models of intermittent swimming assume a higher C_D during a bursting phase than a gliding phase by referring to the Bone-Lighthill boundary layer thinning hypothesis (Weihs 1974; Müller *et al.* 2000; Wu *et al.* 2007; Chung 2009). However, in this study we set C_D to be a *fixed* value for both the bursting and gliding phases of intermittent swimming. This allows us to probe the hypothesis that the energy savings observed in intermittent swimming is not wholly due to the boundary layer thinning hypothesis. In other words, when C_D is fixed regardless of whether a swimmer is oscillating its fin or gliding, then any observed energy savings comes purely from potential flow mechanisms and is not associated with a skin friction rise due to the oscillating fin and/or body. In this study, three different *fixed* drag coefficients, $C_D = [0.005, 0.01, 0.05]$, are used to represent the range of average drag coefficients observed in biology (Videler 1981; Videler & Weihs 1982; Webb *et al.* 1984; Anderson *et al.* 2001; Wu *et al.* 2007; Ehrenstein & Eloy 2013; Ehrenstein *et al.* 2014).

The drag coefficient and the area ratio can be grouped together into a combination parameter known as the Lighthill number (Eloy 2013),

$$Li = C_D S_{wp} \quad (2.1)$$

The Lighthill number characterizes how the body and propulsor geometry affects the balance of thrust and drag forces on a swimmer. For example, for a fixed thrust force and propulsor area during self-propelled continuous swimming, the swimming speed is inversely proportional to the Lighthill number (Moored 2017). If Li is high then a swimmer produces high drag leading to low self-propelled swimming speeds and *vice versa*. In the present study, the Lighthill numbers examined are $Li = [0.04, 0.08, 0.4]$, which fall in a range typical of biology (Eloy 2013).

The virtual body also must be given a mass, m , which can be non-dimensionalized with the added mass of the hydrofoil propulsor, that is,

$$m^* \equiv \frac{m}{\rho S_p c}. \quad (2.2)$$

The non-dimensional mass, m^* , affects not only the acceleration of a swimmer due to any net time-averaged forces over a period, but it also affects the magnitude of the

surging oscillations that occur within a period due to the unsteady forcing of the pitching hydrofoil. Based on the dimensions given to the hydrofoil, the non-dimensional mass becomes a fixed value of $m^* = 3.86$.

The kinematic motion is parameterized with a pitching frequency, f , and a peak-to-peak trailing-edge amplitude, A , reported as a non-dimensional amplitude-to-chord ratio, A/c , and a duty cycle, DC . The amplitude-to-chord ratio is related to the maximum pitch angle, that is, $\theta_0 = \sin^{-1}(A/2c)$. The degree of intermittency of swimming is captured in the duty cycle, which is,

$$DC = \frac{\text{burst period}}{\text{total cycle period}} = \frac{T_{burst}}{T_{cycle}}. \quad (2.3)$$

Figure 2b shows a characteristic pitching signal with the burst, coast and total cycle periods defined. The intermittent signal is a combination of a sinusoidal pitching motion for the burst period and it is followed by a fixed pitch angle of $\theta = 0$ for the duration of the coast period. The total cycle period is simply the addition of the burst and coast periods. The pitching motion about the leading edge of the hydrofoil is then defined as,

$$\theta(t) = \begin{cases} y_s(t) [\theta_0 \sin(2\pi ft)], & 0 \leq t \leq T_{burst} \\ 0, & T_{burst} \leq t \leq T_{cycle} \end{cases} \quad (2.4)$$

$$\text{where } y_s(t) = \begin{cases} -\tanh(m_1 t) \tanh[m_1(t-1)], & DC < 0.9 \\ -\tanh(m_2 t) \tanh[m_2(t-1)], & 0.9 \leq DC \leq 1 \\ 1, & DC = 1 \end{cases} \quad (2.5)$$

This equation defines a reference signal where $0 \leq t \leq T_{cycle}$. The actual signal used in the simulations have N_{cyc} repetitions of this reference signal. Here, $T_{burst} = 1/f$ and $T_{cycle} = T_{burst}/DC$. If $DC = 1$, then the signal (eq. (2.5)) reverts to a continuous sinusoidal signal. In order to obtain discretization independent solutions as the time step size is reduced, the discontinuous angular rates and accelerations at the junction of the burst phase and coast phase must be smoothed. To do this, a hyperbolic tangent envelope function, $y(s)$ is multiplied with the sinusoidal burst signal. This function modifies the slope of the sine wave at $t/T_{Burst} = 0$ and $t/T_{Burst} = 1$ to ensure a smooth connection to the coast phase where m_1 and m_2 constants control the steepness of the connection. In our study, we used $m_1 = 3$ and $m_2 = 1$. Foils are actuated with 9 different duty cycles ranging from 0.1 to 0.9 with 0.1 increments.

2.2. Numerical Methods

To model a high Reynolds (Re) number fluid flow, the field is assumed inviscid, irrotational and incompressible around the hydrofoils. For an incompressible irrotational fluid, if the fluid is considered to be incompressible and irrotational, the continuity equation reduces to the Laplace equation, $\nabla^2 \phi = 0$, where ϕ is the perturbation potential in the fluid domain. In addition, the velocity component normal to the body's surface must be zero (no-flux boundary condition),

$$\nabla \phi \cdot \mathbf{n} = 0 \quad (2.6)$$

where \mathbf{n} is a vector normal to the body's surface, and $\nabla \phi$ is the velocity measured in an inertial frame attached to the undisturbed fluid. The disturbance created by the motion should also decay far from the body (far-field boundary condition),

$$\lim_{r \rightarrow \infty} (\nabla \phi) = 0 \quad (2.7)$$

where $\mathbf{r} = (x, z)$ and \mathbf{v} is the relative velocity between the undisturbed fluid and the body.

Following Katz & Plotkin (2001) and Quinn et. al. (2014), the solution to Laplace's equation can be obtained by distributing elementary solutions (sources and doublets) on the problem boundaries. The elementary solutions of the doublet and source both automatically fulfill the far-field boundary condition (Eq. 2.7). The problem is reduced to finding the strength of the sources and doublets (σ, μ) over known boundaries so that the no-flux boundary condition (Eq. 2.6) is satisfied. One approach to satisfy the no-flux condition indirectly is to use a Dirichlet formulation, that is, we can fix the potential inside the body to be a constant.

To solve the problem numerically, surface S_B is divided into N elements and each element is assigned one collocation point within the body where a constant potential condition is applied to enforce no flux through the element. Prescribing the source strengths to be $\sigma = -\mathbf{n} \cdot (U_\infty + U_{rel})$ where U_{rel} is the velocity of the hydrofoil with respect to an Eulerian frame of reference. This numerical scheme leads to $N + 1$ unknowns (N body doublet strengths and the doublet strength of the first wake element). To solve the linear system, explicit Kutta condition is enforced in the trailing edge. The doublet strength of the first wake panel becomes; $\mu_w = -(\mu_1 - \mu_N)$ where $\mu_1 - \mu_N$ is the vortex strength at the trailing edge and μ_w is the doublet strength of the first wake panel.

At every time step, a panel element with a known doublet strength advects from the trailing edge with the local velocity, rolls up and forms coherent vortices in the wake region. During the rollup process, the ends of the wake doublet elements, which are equivalent to point vortices, must be de-singularized for the numerical stability of the solution. Trajectories of point vortices are discretized as $(x(\Gamma_j), y(\Gamma_j))$ where Γ is the circulation and the trajectories are given by Krasny as (1986),

$$\frac{dx_j}{dt} = \frac{1}{2N} \sum_{k=1}^N \frac{\sqrt{(x_j - x_k)^2}}{\sqrt{((y_j - y_k) - (x_j - x_k))^2 + \delta^2}} \quad (2.8)$$

$$\frac{dy_j}{dt} = \frac{1}{2N} \sum_{k=1}^N \frac{\sqrt{(y_j - y_k)^2}}{\sqrt{((y_j - y_k) - (x_j - x_k))^2 + \delta^2}} \quad (2.9)$$

Equation 2.8 and 2.9 converge to point vortex approximation as $\delta \rightarrow 0$. In the current study, $\delta = 2.5 \times 10^{-4}$ is selected for de-singularization.

The tangential perturbation velocity is found by the local differentiation of the velocity potential. Then the pressure field acting on the body is calculated by using the unsteady Bernoulli equation. The results are collected when the hydrofoil reaches its steady state swimming conditions. The steady state condition is satisfied by a net thrust coefficient criterion, defined as:

$$C_{T,net} = \frac{\overline{T} - \overline{D}}{\rho S_p \overline{U}^2} < 10^{-6} \quad (2.10)$$

To be able to study self-propelled conditions, the velocity of the hydrofoil at the $(n + 1)^{th}$ time step is calculated through forward differencing and the position is calculated using the trapezoidal rule. Following Borazjani et al. 2009,

$$U^{n+1} = U^n + \frac{F_{x,net}^n}{m} \Delta t \quad (2.11)$$

$$x_{LE}^{n+1} = x_{LE}^n + \frac{1}{2}(U^{n+1} + U^n) \Delta t \quad (2.12)$$

where $F_{x,net}^n$ is the net force acting on the hydrofoil in the streamwise direction at the n^{th} timestep, x_{LE} is the leading edge position of the hydrofoil and Δt is the time step.

2.3. Output Parameters and Performance Metrics

Strouhal number which shows, in the context of swimming, the relative magnitude of the width to the length of one cycled shed vortices. It becomes an output from the system since swimming velocity is unknown a priori. Reduced frequency which shows the unsteadiness of the system by comparing spatial wavelength of the shed vortices with the chord length also becomes an output of the system. Strouhal number and reduced frequency are defined as;

$$St = \frac{fA}{U} \quad k = \frac{2\pi fc}{U} \quad (2.13)$$

The force acting on the hydrofoil is calculated by integration of the pressure forces around the hydrofoil. Thrust becomes the streamwise component of the total force acting on the hydrofoil. The thrust and drag forces can be separately calculated with the inviscid, irrotational, incompressible flow assumptions for this free swimming problem. The power input to the fluid is calculated as the inner product of the force vector acting on the hydrofoil with the velocity vector. The propulsive efficiency (η) can be defined as the ratio of useful power output to the power input to the fluid. Another performance metric examined in our study is the cost of transport (CoT). CoT is important because it helps to compare animals of different mass in terms of their energy consumption. CoT and propulsive efficiency are defined as;

$$CoT = \frac{\overline{P}}{\overline{U}m} \quad \eta = \frac{\overline{TU}}{\overline{P}} \quad (2.14)$$

The efficiency in a free swimming problem can be linked to cost of transport. In steady swimming conditions, average thrust of a swimmer equals to average drag. Therefore, thrust can be written as; $\overline{T} = \frac{1}{2}C_d\rho U^2$. Multiplying and dividing CoT relation with thrust yields;

$$CoT = \frac{\frac{1}{2}C_d\rho U^2}{\eta m}$$

This result suggests that at the same free swimming speed, $CoT \propto 1/\eta$.

An important non-dimensional parameter, normalized cost of transport, \hat{CoT} , is introduced for better comparison of intermittently and continuously operating hydrofoils at the same velocity. Similarly, normalized efficiency of the swimmers, $\hat{\eta}$, is defined as the ratio of the efficiencies of two swimming modes at the same velocity. The normalized cost of transport and efficiency are defined as;

$$\hat{CoT} \equiv \frac{CoT_{int}}{CoT_{cont}} \Big|_{\overline{U}} \quad \hat{\eta} \equiv \frac{\eta_{int}}{\eta_{cont}} \Big|_{\overline{U}} \quad (2.15)$$

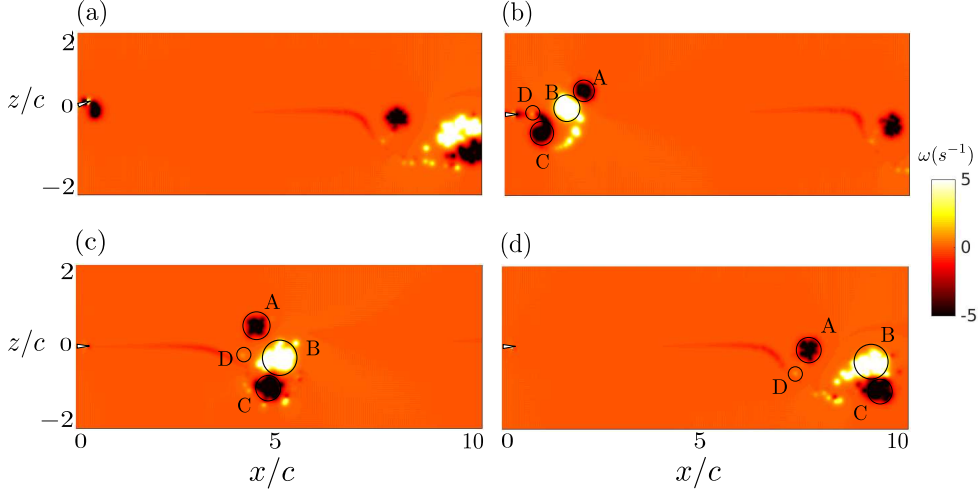


FIGURE 3. Evolution of the vorticity field of an intermittently pitching hydrofoil with $DC = 0.2$, $A/c = 0.7$ and $Li = 0.08$. Four vortices shed per bursting cycle. A, B, C and D vortices represent starting vortex, vortices shed at each time hydrofoil changes the pitching direction and stopping vortex, respectively. Four different snapshots show the evolution of the vortices over one cycle of oscillation: (a) $T_b/4$ (b) T_b (c) $T_c/2$ (d) T_c where T_b represents the bursting period and T_c represents the coasting period.

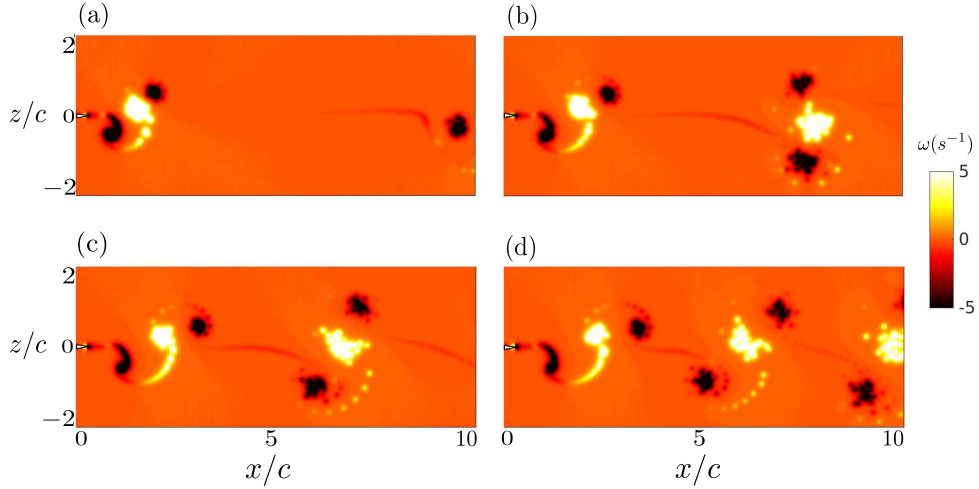


FIGURE 4. Vorticity field comparison of airfoils pitching with $A/c = 0.7$, $Li = 0.08$. Each frame shows another duty cycle; (a) $DC = 0.2$, (b) $DC = 0.4$ (c) $DC = 0.6$, (d) $DC = 0.8$.

3. Flowfield

The maximum amplitude of pitching is restricted to $\theta_0 = 20^\circ$ where wake dynamics is expected to be dominated by the vortices shed from the trailing edge (Walker *et al.* 1985; Carr *et al.* 1977). Figure 3 shows the evolution of the vorticity field throughout a cycle for an intermittent swimmer with $DC = 0.2$. The distribution of positive (anti-clockwise) and negative (clockwise) vorticity is represented with white and black, respectively. There is no near wake at the beginning of the burst period since previous wake structures have advected multiple chord lengths away (Figure 3a). Over each bursting period, four vortices are shed; one starting vortex (vortex A), two of them are the vortices as hydrofoil

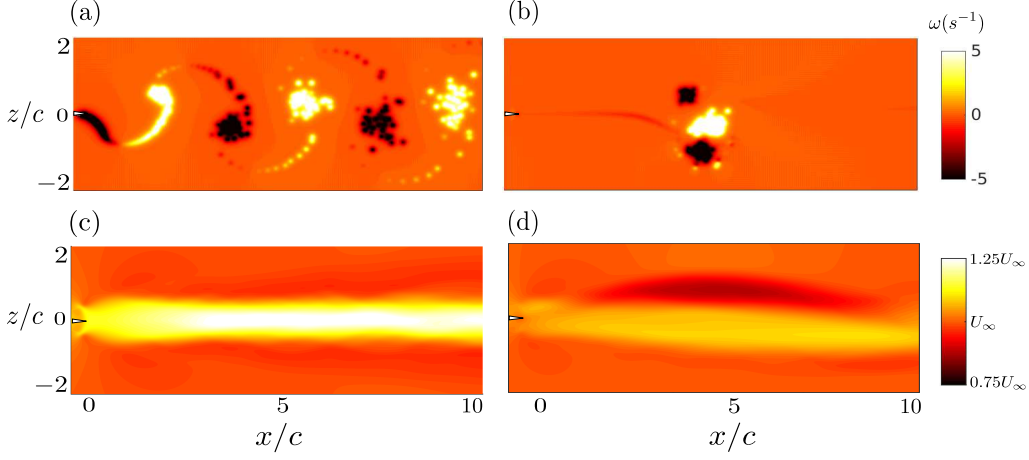


FIGURE 5. The vorticity field of hydrofoils pitching with $A/c = 0.7$ and $Li = 0.08$ at (a) $DC = 1$ and (b) $DC = 0.2$. Time averaged velocity fields of (c) the continuous and (d) the intermittent gait at an average free swimming velocity of 0.14 m/s.

changes direction (vortices B and C) and one weak stopping vortex (D) (Figure 3b). Vortices B and C are stronger and form a pair as they travel downstream (Figure 3c, d). B, C pair induce velocity in the downstream direction which causes the dipole to convect faster than vortices A and D. On the other hand, the induced velocity of vortex A breaks off some part of vortex B and disrupts it. (Figure 3d).

The self-similarity of vortex groups with different duty cycles is shown in Figure 4. For all $DC = 0.2, 0.4, 0.6, 0.8$ cases, four vortices are shed per bursting period. As described above for $DC = 0.2$ case, the vortex shedding pattern and the evolution of the vortices are very similar regardless of the duty cycle. However, the spacing of the vortex groups change with variation in the duty cycle. As the duty cycle is increased the vortex groups become more tightly packed.

The self similarity observed in vortex groups shed from the intermittently pitching hydrofoils are broken for the limiting case of continuous swimming (Figure 5a). Unlike an intermittently pitching hydrofoil (Figure 5b), continuous swimmer, as documented in the literature by Freymuth (1988) and Koochesfahani (1989), produces a reverse von Kármán vortex street where two vortices are shed per pitching period.

The asymmetrical strength of the four vortices in the intermittently pitching hydrofoil's wake is also reflected in the time-averaged jets. Figure 5c-d show the comparison of a continuously pitching hydrofoil with its intermittently pitching counterpart at $DC = 0.2$ at the same free swimming velocity of $U = 0.14$ m/s. For the continuous gait, the symmetrically shed vortices create a reverse von Kármán street which leads to one strong jet. For the intermittently swimming hydrofoil, in the near wake ($x/c \leq 1$), the vortices are shed in a similar manner to a classic reverse von Kármán creating a time-averaged momentum jet in the downstream direction. In the far wake ($x/c \geq 1$), the three strong vortices evolve into two pairs, with one pair inducing a velocity in the downstream direction, while the other induces a velocity upstream. In time-averaged sense this creates a momentum surplus and deficit region that are parallel to each other.

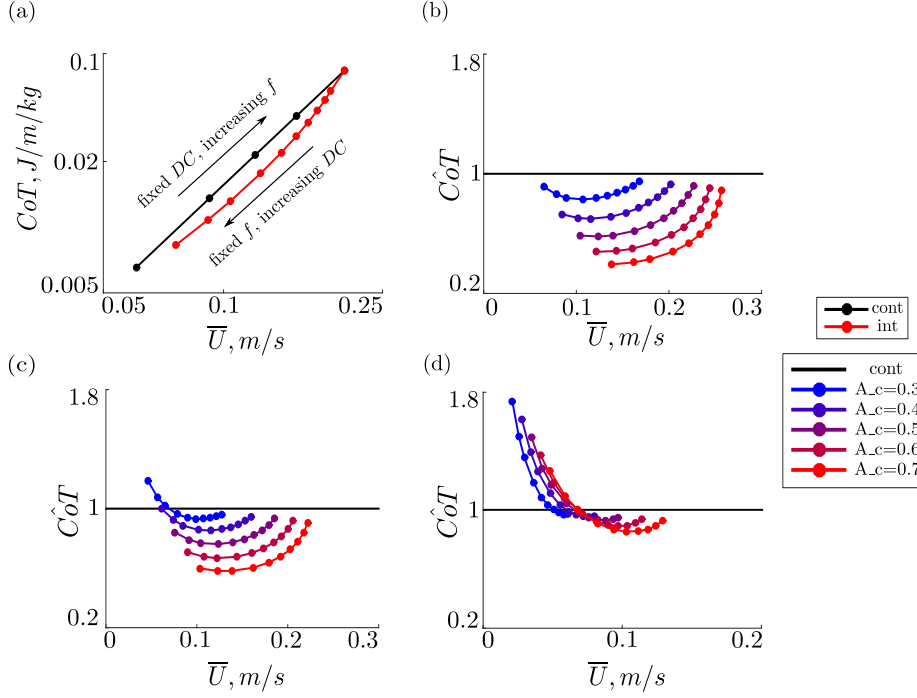


FIGURE 6. (a) Cost of Transport as a function of average free swimming speed comparison of continuously and intermittently swimming airfoils at $A/c = 0.5$ for a fixed drag coefficient of $Li = 0.08$ (b), (c), (d) \hat{CoT} as a function of average free swimming speed of continuously and intermittently swimming airfoils for 3 different fixed drag coefficients; $Li = 0.04$, $Li = 0.08$, $Li = 0.4$, respectively.

4. Performance Comparison

In Figure 6a, the CoT values is plotted as a function of the swimming velocity on a log-log scale graph for $A/c = 0.5$. The continuous swimmer has a fixed duty cycle, $DC = 1$, and pitches with various frequencies in the range of 0.2 Hz – 1 Hz. On the other hand, the intermittent swimmer has a fixed frequency, $f = 1$ Hz (frequency is defined only over the bursting period for intermittent gait), and the duty cycle is varied in between $DC = 0.1 - 1$. At $DC = 1$ and $f = 1$ Hz, the intermittent and continuous swimmers are equivalent. When the duty cycle is lowered, the swimming velocity consequently drops and at the same time the CoT decreases. It can be observed that by using an intermittent over continuous gait, swimmers can lower their CoT while maintaining their swimming speed, albeit with an increase in the oscillation frequency during the burst period. Importantly, this benefit is observed with potential flow simulations that do not compute the skin friction from the boundary layer and instead rely on a drag law with a fixed drag coefficient. This means that the observed benefit cannot be due to the Bone-Lighthill boundary layer thinning hypothesis (Lighthill 1971), a viscous mechanism, but instead must be due to an inviscid mechanism. This leads to a host of questions such as, how much of a benefit is observed? To what range of parameters does this benefit extend? What is the inviscid mechanism? To answer these questions, a wide range of data is shown in the other graphs of Figure 6.

Figures 6b-d show the normalized cost of transport as a function of the mean swimming speed for three different Lighthill numbers, that is, $Li = 0.04$, 0.08 , and 0.4 . The normalized cost of transport compares the CoT of an intermittent swimmer to that of

a continuous swimmer at the same swimming speed. If $C\hat{o}T > 1$ then a continuous swimming gait is energetically beneficial. If $C\hat{o}T = 1$ then both gaits are energetically equivalent. Finally, if $C\hat{o}T < 1$ then an intermittent gait is energetically beneficial. Having a $C\hat{o}T$ value smaller than one means choosing intermittent swimming is more economical than swimming continuously. Regardless of the Li , choosing intermittent swimming is energetically more favorable as the amplitude of pitching increases. Additionally, the available energetic benefit from intermittent swimming becomes greater for decreasing Li of swimmers. In fact, at $Li > 0.4$ there is essentially a negligible energetic savings only at very high duty cycles that can be garnered by switching to an intermittent gait. Based on the drag coefficient of the laminar boundary layer on a flat plate $C_D = 0.664 Re_l^{-1/2}$ and the area ratio of $S_{wp} = 8$, then $Li = 5.312 Re^{-1/2}$ and the condition on Li can be cast into a condition on the Reynolds number such that $Re > 175$ must occur for there to be an observable energetic benefit for intermittent swimming. At least this is the case for the inviscid benefit of intermittent swimming, however, a Bone-Lighthill viscous benefit is not restricted in the same manner.

The lower bound on Re where an intermittent benefit can be observed is reflected in biological studies. Larval northern anchovy uses continuous swimming whereas adult northern anchovy use an intermittent swimming mode (Weihs 1980). As larval northern anchovy reaches < 5 mm long, which corresponds to a $Re \approx 100$, intermittent motion becomes more economical and larva starts to intersperse coasting and accelerating. Similarly, Muller et al. (2000) conducted two dimensional particle image velocimetry experiments to study the flow fields of larval and adult northern anchovy. The recorded larval Re numbers for burst periods are in between 10 and 100 whereas adult Re numbers are on the order of 5000. They concluded that the viscous forces are more important in compared to the propulsive forces as Reynolds number (Re) is on the order of 10. However, as anchovy grows larger, inertial forces become more important than the viscous forces and after a threshold Re , choosing intermittent swimming is more favorable over continuous swimming for the anchovy.

For the lowest Li and highest amplitude examined in this study, the CoT reduction is as high as 60%. In other words, a swimmer can choose to swim intermittently rather than continuously and save as much as 60% of its energy per unit mass to travel a unit distance. Importantly, unlike previous studies, this conclusion is obtained by fixing the drag coefficient for both bursting and coasting periods of swimming, meaning that the observed benefit is not only due to the Bone-Lighthill boundary layer thinning hypothesis, but there is also an inviscid mechanism that leads to energy savings when a swimmer uses an intermittent gait.

5. Inviscid Energy Saving Mechanism and Scaling Laws

To investigate the mechanism behind the intermittent swimming benefit, thrust generation over an active period is plotted for intermittently and continuously pitching airfoils (see Figure 7). All intermittent cases, on average, generate more thrust than their continuous counterparts, operating with the same amplitude-to-chord ratio. Although thrust generation phases, positive halves of the curves, are similar in terms of magnitude for both modes of swimming, intermittent swimmers experience less drag. The experienced drag difference between intermittent and continuous swimmers is increasing with increasing amplitude and decreasing drag coefficient. In other words, choosing intermittent swimming for higher amplitudes and lower coefficient of drags lead to better thrust generation performance over continuous swimming.

The induced drag effect with changing duty cycle can be explained by studying the

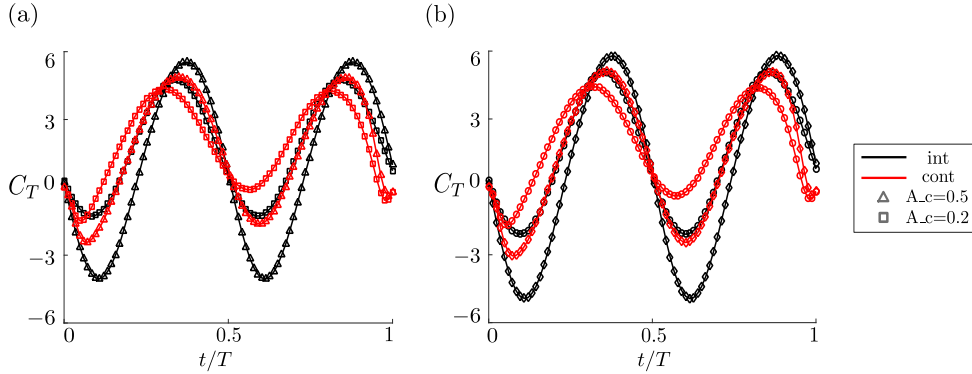


FIGURE 7. (a) Coefficient of thrust as a function of one bursting cycle for continuously and intermittently swimming airfoils. Foils operate at $DC=0.2$ and $A/c = 0.2, 0.5$ (a) $Li=0.04$ (b) $Li=0.08$

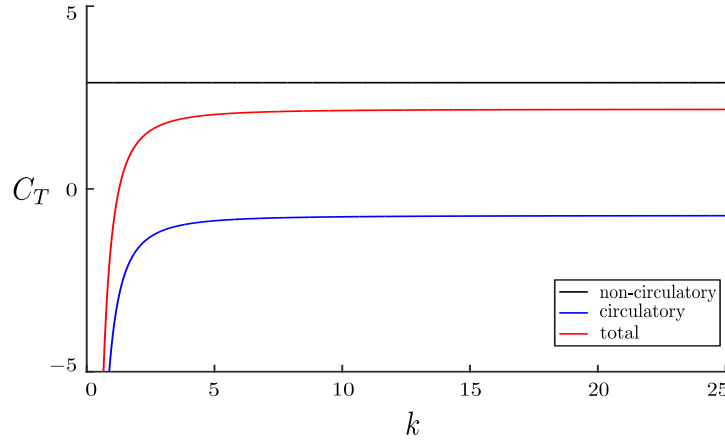


FIGURE 8. Garrick's analytic solution for total thrust coefficient and its decomposition into circulatory and non-circulatory parts

analytical model proposed by Garrick (1937) which estimates the average thrust production of a two dimensional oscillating plate. As originally stated by Knoller (1909) and Betz (1912), thrust is proportional to lift for an oscillating airfoil. Therefore, Garrick divided the total thrust into two components similar to the analytic solution of total lift of an oscillating thin airfoil proposed by Theodorsen (1935); a non-circulatory part and a circulatory part. The general form of the thrust coefficient, when time averaged thrust is normalized by the non-circulatory term, becomes only a function of reduced frequency (see Figure 8). Decomposing the non-circulatory and circulatory parts leads to a constant term and a reduced frequency depended term, respectively. The non-circulatory term generates thrust for all reduced frequency values whereas circulatory term induces drag. The important observation is by changing duty cycle, a swimmer control its reduced frequency, independent of any other input parameters. In other words, by changing duty cycle, swimmer can control the ratio of the induced drag generating circulatory forces to thrust producing non-circulatory forces.

Thrust is not non-dimensionalized using the dynamic pressure as in a steady static airfoil case. As Dewey et al. noted (2013), added mass forces perpendicular to the pitching direction scales with the characteristic mass $\rho c^2 b$ and the characteristic acceleration $f^2 A$. Taking the streamwise component in small angle approximation, added mass forces

scales as $\rho S_p f^2 A^2$, where S_p is the planform area of the propulsor. On the other hand, streamwise circulatory forces, which in this case drag, scales as $D_i \approx L \alpha_i \propto \rho S_p U^2 \alpha_e \alpha_i$ and $D_i \propto \rho S_p U^2 (\theta - \alpha_i) \alpha_i$ where L is lift force, α_i is the induced angle of attack and α_e is the effective angle of attack. The induced angle of attack, α_i , scaling can be found considering the shed circulation over one oscillating period. Then, upwash/downwash produced by the wake vorticity is determined by using Biot Savart law. Now, the induced drag forces scales as $D_i \propto \rho S_p f^2 A^2 f(k)$ where $f(k)$ is a function of reduced frequency. The added mass and induced drag components are generated over the bursting period. To account for the intermittency, duty cycle is introduced to the total thrust relation,

$$\overline{T} = DC \left[C_{T0} \rho S_p f^2 A^2 - C_{Di} \rho S_p f^2 A^2 f(k) \right]$$

The $DC \rho S_p f^2 A^2$ term is precisely the non-circulatory term in the analytic solution of Garrick's model with the modification of the duty cycle effect. Non-dimensionalizing the total thrust with this term makes the thrust coefficient equation similar to the Garrick relation which is only a function of reduced frequency,

$$C_T(k) = \frac{\overline{T}}{DC \rho S_p f^2 A^2} = C_{T0} - C_{Di} f(k)$$

Similarly, scaling for the power input to the fluid is divided into two components; small amplitude motion and large amplitude motion. For small amplitude motion, moment on the foil scales with lift force and the chord length, Lc , and power input scales as $Lc\dot{\theta}$. Working this expression out gives $\rho S_p U_\infty f^2 A^2$ for small amplitude motion power scaling. For large amplitudes, unsteady pressure difference is more important across the flapping airfoil. Normal force, F_N , across the foil scales as $\rho S_p (c\dot{\theta})^2$ and power input scales as $F_N(c\dot{\theta})$. Working out this expression gives for large amplitude power scaling as $\rho S_p f^3 A^3$. Total power input to the fluid after introducing duty cycle becomes,

$$\overline{P} = DC \left[C_{Ps} \rho S_p U_\infty f^2 A^2 + C_{Pl} \rho S_p f^3 A^3 \right]$$

where C_{Ps} is the small amplitude power coefficient and C_{Pl} is the large amplitude power coefficient. The new power relation suggests that with a given linear velocity of the airfoil which scales with fA , regardless of the individual values of frequency and amplitude, you would predict the same power input to the fluid. However, as the amplitude of pitching becomes smaller, the shed vortices squeeze closer to the airfoil. Although the fA multiplication is constant, proximities of vortex groups for different amplitudes of pitching changes the power input to the fluid. To account for this phenomenon, large amplitude part of the power relation is modified with $(A/c)^n$. Therefore, the modified power equation becomes,

$$\overline{P} = DC \left[C_{Ps} \rho S_p U_\infty f^2 A^2 + C_{Pl} \frac{\rho S_p f^3 A^3}{(A/c)^n} \right]$$

where $n=0.25$. Non-dimensionalizing the total power input with the small amplitude power scaling gives us;

$$C_P(St^*) = \frac{\overline{P}}{DC \rho S_p f^3 A^3} = C_{Ps} + C_{Pl} St^*$$

leaving the power coefficient as only a function of modified Strouhal number defined as $St^* = St/(A/c)^n$.

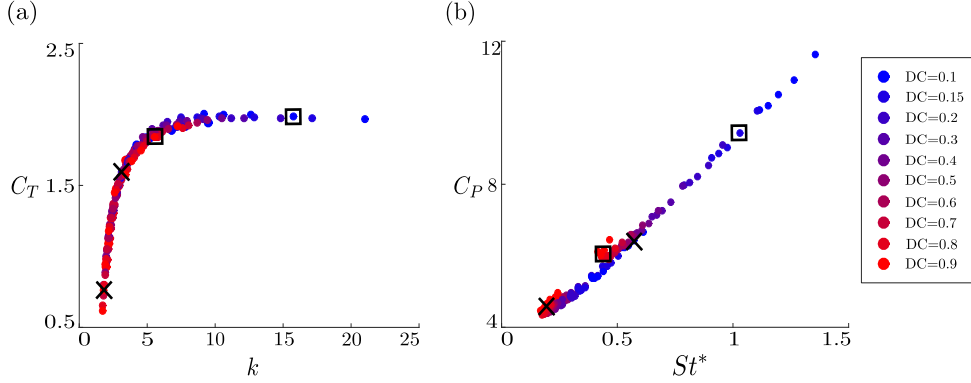


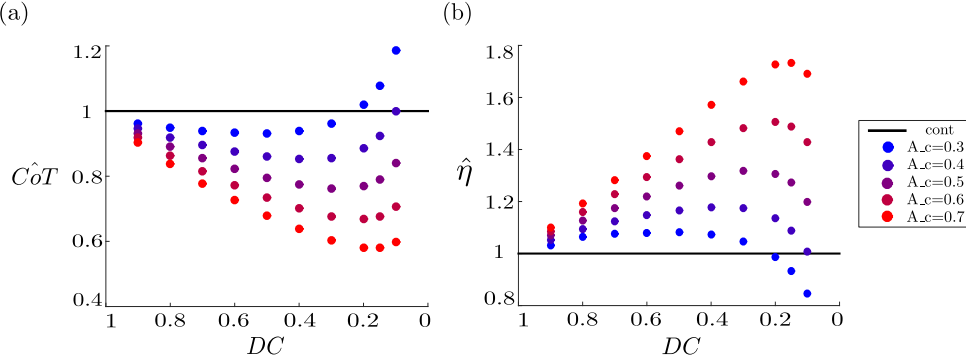
FIGURE 9. (a) Average thrust coefficient as a function of reduced frequency. (b) Average power coefficient as a function of St^* . The parameter range of data is $DC \rightarrow 0.1 - 0.9$, $A_c \rightarrow 0.3 - 0.7$, $Li \rightarrow 0.04 - 0.2$

Figure 9a shows the coefficient of thrust, reduced frequency relationship for intermittent swimmers operating with varying amplitude-to-chord ratios, drag coefficients and duty cycles. Collapse of data to a single curve highlights the dependence of coefficient of thrust to only reduced frequency. Decreasing duty cycle leads to a decrease in cruising velocity and consequently increases reduced frequency. Therefore, a swimmer can decrease its duty cycle and significantly increase its coefficient of thrust especially in the reduced frequency range of 2 to 5. As described in the Garrick's analytic solution, although physically induced drag increases as reduced frequency increases, the rate of increase of thrust producing added-mass forces is larger than the rate of increase of induced drag forces. Therefore, the ratio of added-mass thrust forces to induced drag forces grows larger until the ratio asymptotes to a constant value as $k \rightarrow \infty$.

Power coefficient as a function of St^* relationship is shown in Figure 9b. Decent collapse of data confirms the St^* dependence of power coefficient with the new unsteady scalings. Changing duty cycle affects the St^* similar as in reduced frequency case. Decreasing duty cycle increases the St^* and so the power coefficient. One important observation is unlike thrust coefficient reduced frequency relationship, power coefficient increase rate is a linear function of St^* .

To understand the efficiency, the thrust and power coefficients should be considered together. Although the unsteady scalings are different than the classical scalings, the ratio of thrust coefficient to power coefficient still leads to propulsive efficiency. Therefore different rate of change of thrust and power coefficients with duty cycle could be exploited in a way to maximize efficiency. For example, the black cross and rectangle pairs in Figure 10(a) and (b) represents the duty cycle change from 0.9 to 0.2 for the same input parameter set. For smaller range of reduced frequency and St^* , decrease in duty cycle leads to a higher rate of increase in thrust coefficient in compared to the power coefficient. This sharp jump of coefficient of thrust also increases the efficiency of swimming. However, as black rectangles exemplify, after a certain reduced frequency, thrust coefficient asymptotes to a value while power coefficient continues to increase as a linear function of St^* .

The efficiency in a free swimming problem can be linked to cost of transport. In steady swimming conditions average thrust equals to average drag. Therefore, thrust can be

FIGURE 10. (a) C_oT and (b) $\hat{\eta}$ as a function of decreasing duty cycle

written as; $\overline{T} = \frac{1}{2}C_d\rho U^2$. Multiplying and dividing CoT relation with thrust yields;

$$CoT = \frac{\frac{1}{2}C_d\rho U^2}{\eta m}$$

This result suggests that at the same free swimming speed, $CoT \propto 1/\eta$. The $\hat{\eta}$ behavior with changing duty cycle can now be studied similar to C_oT , where $\hat{\eta}$ is the normalized efficiency of intermittently swimming airfoils with the continuously swimming ones at the same swimming speed; $\hat{\eta} = \eta_{int}/\eta_{cont}$. Since the C_oT and $\hat{\eta}$ are inversely proportional to each other, as C_oT decreases, $\hat{\eta}$ increases (see Figure 10). Further drop in duty cycle pushes the reduced frequency values above 5 and power increase surpasses thrust rise which leads to a decrease in $\hat{\eta}$ and an increase in C_oT values.

The scaling relations for free swimming velocity and C_oT are also studied. Using previously found thrust scaling and taking advantage of thrust equals drag in a free swimming problem, velocity relation becomes,

$$U_{scaling} = fA\sqrt{2DC\frac{C_T(k)}{C_dS_{wp}}}$$

and using free swimming velocity and power relations, C_oT scalings becomes;

$$C_oT_{scaling} = \frac{\left[f^2A^2[C_{Ps}U_\infty + C_{Pl}fA(A/c)^{-n}]\right]_{int}}{\left[f^2A^2[C_{Ps}U_\infty + C_{Pl}fA(A/c)^{-n}]\right]_{cont}}$$

New variables R_U and R_{C_oT} are introduced to compare the predicted values from the scaling laws and the results from the computations where $R_U = U_{scaling}/U_{computation}$ and $R_{C_oT} = C_oT_{scaling}/C_oT_{computation}$. Both scaling laws for free swimming velocity and C_oT match remarkably well with the computational results (see Figure 11). Scaling relation for velocity predicts the computational result within 3% of error range while scaling law for the C_oT predicts within 6%.

6. Conclusion

In conclusion, starting with Lighthill's boundary layer thinning hypothesis (Lighthill 1971), intermittent swimming benefit has been linked to the rise of skin friction drag in swimming. However, our analysis, which only includes pressure forces, concludes that for

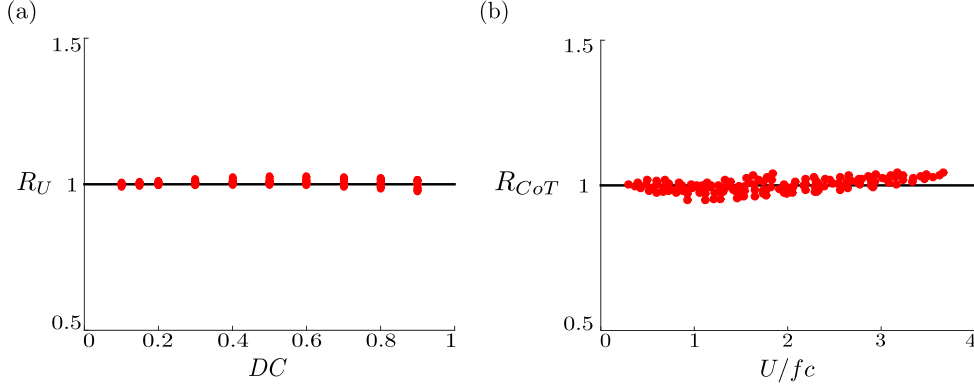


FIGURE 11. (a) Ratio of the free swimming velocity predicted with the scaling laws and the computational results as a function of duty cycle (b) Ratio of $\hat{C}\omega T$ predicted with the scaling laws and the computational results as a function of duty cycle

pure pitching motion, an inviscid energy saving mechanism is also in play. It is observed that for low Lighthill number and high amplitude pitching cases, introducing intermittency saves up to 60% more energy in compared to continuously pitching airfoils at the same free swimming velocity.

It is observed that four vortices per pitching cycle are shed for intermittent swimmers regardless of the duty cycle. Since every pitching period is combined with a coasting period, on top of the two vortices shed once the hydrofoil changes pitching direction, a starting and a stopping vortex are shed in the beginning and at the end of the pitching period. The time average velocity field of an intermittent swimmers' wake is asymmetric. A high intensity jet is tilted downward and there is a deficit region on top of the jet.

One of the key discoveries is; unlike continuous swimmers, intermittent swimmers can directly change its reduced frequency and St^* independent of any other parameters by adjusting duty cycle. A continuous swimmer with low coefficient of drag and high amplitude of pitching operates at a reduced frequency range of 2-5 and a St^* range of 0.15-0.5. Introducing intermittency on these swimmers increases the thrust generation and the rate of change of thrust is more than the power input to the fluid which therefore leads to a net increase in propulsive efficiency.

The thrust change mechanism is explained using the Garrick's analytical model (1937). Garrick divided the total thrust forces into non-circulatory and circulatory parts. Regardless of the reduced frequency range, non-circulatory forces always generate thrust. On the other hand, circulatory forces induces drag and the proportion of induced drag to non-circulatory or added mass forces is decreasing with increasing reduced frequency in the reduced frequency range of 2-5. Therefore, as the reduced frequency is adjusted in the range of 2-5, particularly by decreasing duty cycle, induced drag forces become smaller proportional to the added mass forces which leads to a net increase in the total thrust production. However, after a certain reduced frequency the proportion of added mass to induced drag forces saturates to a constant value. Therefore, further increase of reduced frequency does not change the total net thrust production.

Power scalings are studied by linearly superposing two extremes of motion; small amplitude and large amplitude. For small amplitude motion, characteristic force becomes the lift force but for large amplitude extreme, unsteady pressure difference across the airfoil is important. Furthermore, an amplitude modification is made to the large ampli-

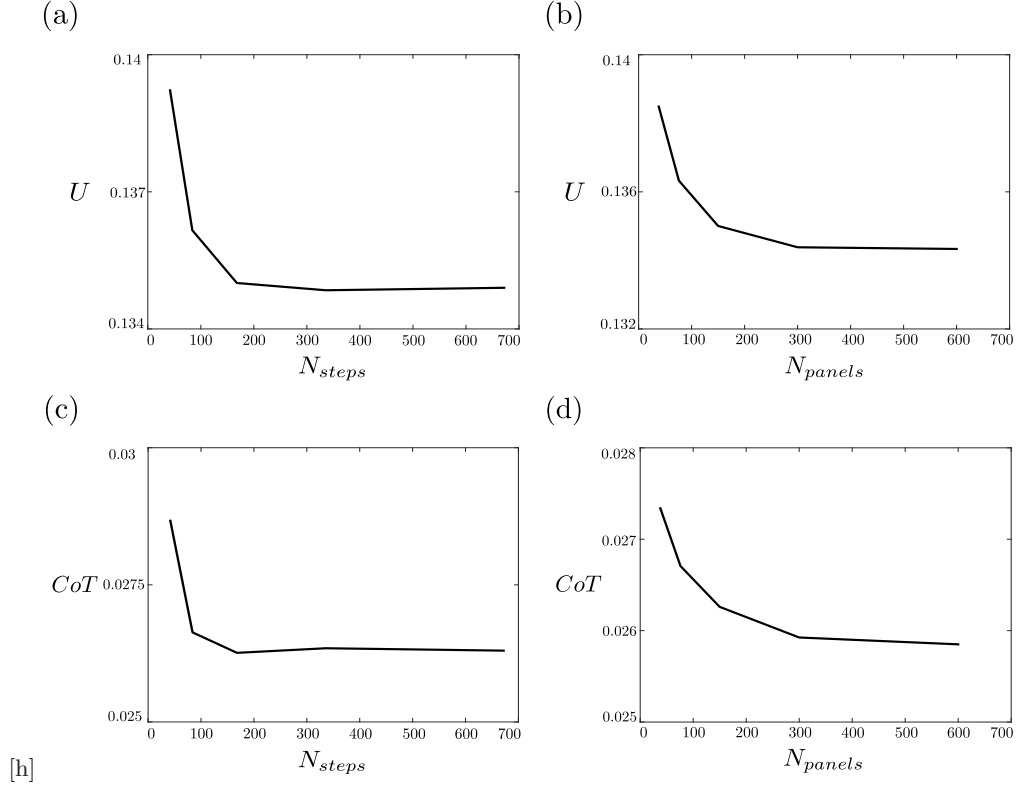


FIGURE 12.

tude part of the scaling relations to account for different vortex proximities for different amplitudes of pitching.

Our study forces the separation to happen from the trailing edge and flow is attached all over the airfoil surface. Therefore, we tried to limit our parameter set for no separation range documented in the literature. The study of the full viscous effects are subject to future work. Viscous studies would help us to understand the actual parameter range where intermittent swimming is beneficial over continuous swimming as well as it would dissect the contribution of each viscous/inviscid energy saving mechanisms.

Acknowledgments

This work was funded by the Office of Naval Research under Program Director Dr B. Brizzolara, MURI Grant Number N00014-14-1-0533.

Appendix A Convergence study

Convergence studies found that the free-swimming velocity and cost of transport is tracked while doubling the number of body panels and the number of time steps per bursting phase of the cycle as shown in Figure 13. The computations are run for 8 pitching cycles and the time averaged data are obtained by averaging over the last cycle. The change in between the seventh and eight cycles in free swimming velocity and cost of transport was less than 1%. For practical purposes an example case is shown in Figure

14. The parameter set used for this particular study is; $c=0.07\text{m}$, $C_d=0.01$, $A/c=0.5$, $f=1\text{Hz}$, $DC=0.5$.

REFERENCES

- ANDERSON, E. J., MCGILLIS, W. R. & GROSENBAUGH, M. A. 2001 The boundary layer of swimming fish. *The Journal of experimental biology* **204** (Pt 1), 81–102.
- BEAMISH, H. W. F. 1966 Swimming endurance of some Northwest Atlantic fishes. *Journal of the Fisheries Board of Canada* **3** (3).
- BETZ, A. 1912 *Ein beitrage zur erklerung des segelfluges*.
- BORAZJANI, I. & SOTIROPOULOS, F. 2009 Numerical investigation of the hydrodynamics of anguilliform swimming in the transitional and inertial flow regimes. *The Journal of experimental biology* **212** (Pt 4), 576–592.
- CARR, L. W., MCALISTER, K. W. & MCCROSKEY, W. J. 1977 Analysis of the Development of Dynamic Stall Based on Oscillating Airfoil Experiments. *Tech. Rep.*.
- CHUNG, M-H. 2009 On burst-and-coast swimming performance in fish-like locomotion. *Bioinspiration & Biomimetics* **4** (3), 036001.
- DEWEY, P. A., BOSCHITSCH, B. M., MOORED, K. W., STONE, H. A. & SMITS, A. J. 2013 Scaling laws for the thrust production of flexible pitching panels. *Journal of Fluid Mechanics* **732**, 29–46.
- EHRENSTEIN, U. & ELOY, C. 2013 Skin friction on a moving wall and its implications for swimming animals. *Journal of Fluid Mechanics* **718**, 321–346.
- EHRENSTEIN, U., MARQUILLIE, M. & ELOY, C. 2014 Skin friction on a flapping plate in uniform flow. *Philosophical transactions. Series A, Mathematical, physical, and engineering sciences* **372** (2020), 20130345–.
- ELOY, C. 2013 On the best design for undulatory swimming. *Journal of Fluid Mechanics* **717** (2013), 48–89.
- FREYMUTH, P. 1988 Technical Notes **26** (7), 881–883.
- GARRICK, I. 1937 Propulsion of a Flapping and Oscillating Airfoil. *Tech. Rep.*.
- KATZ, J. & PLOTKIN, A. 2001 *Low Speed Aerodynamics*. McGraw-Hill, Inc.
- KNOLLER, R. 1909 Die gesetze des luftwiderstandes. *Osterreichischer Flugtechnischen Vereines*.
- KOOCHESFAHANI, M. M. 1989 Vortical patterns in the wake of an oscillating airfoil. *AIAA Journal* **27** (9), 1200–1205.
- KRASNY, R. 1986 A study of singularity formation in a vortex sheet by the point-vortex approximation. *Journal of Fluid Mechanics* **167** (-1), 65.
- LIGHTHILL, M. J. 1971 Large-Amplitude Elongated-Body Theory of Fish Locomotion. *Proceedings of the Royal Society B: Biological Sciences* **179** (1055), 125–138.
- MARAIS, C., THIRIA, B., WESFREID, J. E. & GODOY-DIANA, R. 2012 Stabilizing effect of flexibility in the wake of a flapping foil. *Journal of Fluid Mechanics* **710** (September), 659–669.
- MÜLLER, U. K., STAMHUIS, E. J. & VIDELER, J. J. 2000 Hydrodynamics of unsteady fish swimming and the effects of body size: comparing the flow fields of fish larvae and adults. *The Journal of experimental biology* **203** (Pt 2), 193–206.
- MUNSON, B. R. 1990 *Fundamentals of fluid mechanics*.
- QUINN, D. B., MOORED, K. W., DEWEY, P. A. & SMITS, A. J. 2014 Unsteady propulsion near a solid boundary. *Journal of Fluid Mechanics* pp. 152–170.
- RIBAK, G., WEIHS, D. & ARAD, Z. 2005 Submerged swimming of the great cormorant *Phalacrocorax carbo sinensis* is a variant of the burst-and-glide gait. *The Journal of experimental biology* **208** (Pt 20), 3835–49.
- THEODORSEN, T. 1935 General Theory of Aerodynamic Instability and the Mechanism of Flutter. *Tech. Rep.*.
- VIDELER, J. J. 1981 Swimming Movements, Body Structure and Propulsion in Cod *Gadus morhua*. *Symp. zool. Soc. Lond.* (48), 1–27.
- VIDELER, J. J. & WARDLE, C. S. 1991 Fish swimming stride by stride: speed limits and endurance. *Reviews in Fish Biology and Fisheries* **1** (1), 23–40.

- VIDELER, J. J. & WEIHS, D. 1982 *Energetic Advantages of Burst-and-Coast Swimming of Fish At High Speeds*.
- WALKER, J. M., HELIN, H. E. & STRICKLANDJ, J. H. 1985 An Experimental Investigation of an Airfoil Undergoing Large-Amplitude Pitching Motions. *AIAA Journal* **23** (8), 1141–1142.
- WEBB, P. W. 1975 *Hydrodynamics and energetics of fish propulsion*.
- WEBB, P. W., KOSTECKI, P. T. & STEVENS, E. D. 1984 The effect of size and swimming speed on locomotor kinematics of rainbow trout. *Journal of Experimental Biology* **109** (1), 77–95.
- WEBBER, D. M., BOUTILIER, R. G., KERR, S. R. & SMALE, M. J. 2001 Caudal differential pressure as a predictor of swimming speed of cod (*Gadus morhua*). *The Journal of experimental biology* **204** (Pt 20), 3561–3570.
- WEIHS, D. 1974 Energetic advantages of burst swimming of fish. *Journal of Theoretical Biology* **48** (1), 215–229.
- WEIHS, D. 1980 Energetic significance of changes in swimming modes during growth of larval anchovy *Engraulis mordax*. *Fishery Bulletin* **77** (3), 597–604.
- WU, G., YANG, Y. & ZENG, L. 2007 Kinematics, hydrodynamics and energetic advantages of burst-and-coast swimming of koi carps (*Cyprinus carpio koi*). *The Journal of experimental biology* **210** (Pt 12), 2181–2191.